JOURNAL OF PROPULSION AND POWER
Vol. 17, No. 4, July–August 2001

Computation of Hall Thruster Performance

L. Garrigues*
Université Paul Sabatier, 31062 Toulouse Cedex 4, France
I. D. Boyd†
University of Michigan, Ann Arbor, Michigan 48109
and
J. P. Boeuf‡
Université Paul Sabatier, 31062 Toulouse Cedex 4, France

A quasi-neutral one-dimensional hybrid model of a stationary plasma thruster has been used to predict the performance of a laboratory model thruster tested in the Propulsion Ionique pour Vols Orbitaux, Interprétation et Nouvelles Expériences, facility. In this model ions are treated as particles and electrons as a fluid and quasi neutrality is assumed. We describe the calculated efficiencies, thrust, and specific impulse using xenon and krypton as propellant and their variations as a function of applied voltage and mass flow rate. Typically, for a voltage of 350 V and an anode mass flow rate of 5 mg/s, the thrust is on the order of 75 mN for xenon and krypton, and the global efficiency is 40 and 30%, respectively, for xenon and krypton. Although the model is rather simple, the predicted trends are in reasonable agreement with the experimental measurements. The question of doubly charged ions is also examined, and results show that they do not strongly contribute to performance in a stationary plasma thruster-100 Hall thruster.

Nomenclature

A	=	area cross section of the thruster, m^2
B	=	magnetic field, T
C^α	=	ion production term, $m^{-3}s^{-1}$
d	=	dimension of the channel, m
E	=	electric field, Vm^{-1}
e	=	electric charge constant, 1.602×10^{-19} C
f_i^α	=	ion distribution function
g	=	gravitational constant, 9.81 ms^{-2}
I_{sp}	=	specific impulse, s
J_i^α, J_i, J_d	=	singly and doubly charged ion, total ion, and discharge currents, A
k_i^+, $k_i^{g,\alpha}$, k_m	=	ionization from single ion and from ground state and momentum exchange rates, m^3s^{-1}
k_ε^+, k_ε^g	=	electron energy loss rates from singly charged ion and from ground state, m^3s^{-1}
m_e, M	=	electron mass, 9.1×10^{-31} kg; neutral atom mass Xe = 131.3 UMA and Kr = 83.8 UMA
$\dot{m}$, $\dot{m}_i^\alpha$	=	propellant mass flow rate at the anode and ion mass flow rate at the exhaust, $kg \cdot s^{-1}$
N_j^α, N_s^α, N_m^α	=	number of macroparticles created in a cell j, simulated, and minimal
n_i^α, n_p, N_a	=	ion, plasma, and neutral densities, m^{-3}
P_d	=	dissipated power, W
$\boldsymbol{r}_l$, $\boldsymbol{v}_l$, w_l	=	position, m; velocity, ms^{-1}; and weight of a test particle
S_j^α, $S_{\max}^\alpha$	=	ion production rate in a cell j and maximal ion production rate, $m^{-3}s^{-1}$
$S^{g,\alpha}$, S^+	=	ion production rates from ground state and from singly charged ion, $m^{-3}s^{-1}$
T, T_i^α	=	total, singly and doubly charged ion thrust, N
V_d	=	applied voltage, V
$\overline{v_e}$, v_i^α, v_0	=	electron, ion, and neutral atom velocities, ms^{-1}
x, v_x	=	axial position, m; axial velocity, ms^{-1}
Z_α	=	ionicity
α	=	single- and double-charged ions, 1, 2
β_T, β_φ	=	ratio of thrust and ion flux
γ	=	thrust loss factor
Δt	=	ion transport time step, s
δ	=	Dirac function
$\overline{\varepsilon_e}$, ε_b	=	electron mean energy and average beam ion energy, eV
η, η_u, η_a, η_E	=	total, propellant, acceleration, and beam energy efficiencies
μ_e	=	axial electron mobility, $m^2V^{-1}s^{-1}$
ν_i^+, ν_i^α	=	frequencies of ionization from singly charged ion and from ground state, s^{-1}
ν_m, $\nu_{\text{wall},\,m}$	=	frequencies of momentum exchange collision and collisions with walls, s^{-1}
$\overline{\nu_\varepsilon}$	=	total electron energy loss frequency, s^{-1}
φ_i^α, Φ_0	=	ion flux and neutral flux in the anode plane, $m^{-2}s^{-1}$
ω_B	=	electron angular cyclotron frequency, s^{-1}

Introduction

IN a stationary plasma thruster (SPT), the ions are created and accelerated in a plasma channel concentrated between two concentric dielectric cylinders. Xenon (or krypton) is injected through the anode located at one end of the channel. The cathode is outside the channel and provides the electron current entering the channel through the other end of the channel (exhaust). Because of the low gas pressure in the channel and the small dimensions of the device, a plasma can be created in the channel only if the electrons are confined by a magnetic field. A radial magnetic field is created in the channel by external coils and a magnetic circuit. The radial magnetic field is large in the exhaust region and decreases toward the anode. The large value of the radial magnetic field in the exhaust region induces a drop of the axial electron velocity. To maintain large enough plasma conductivity, the axial electric field must increase in the exhaust region. Electron heating in this field leads to strong ionization of the neutral flow. The ions, which are not sensitive to the magnetic field in the channel, are accelerated by the electric field in the exhaust region.

Received 22 January 2000; revision received 13 December 2000; accepted for publication 8 Febuary 2001.

*Postdoctoral Research Associate, Centre de Physique des Plasmas et Applications de Toulouse, 118 route de Narbonne. Member AIAA.

†Associate Professor, Department of Aerospace Engineering. Senior Member AIAA.

‡Research Scientist at CNRS, Centre de Physique des Plasmas et Applications de Toulouse, 118 route de Narbonne. Member AIAA.

The thrust and specific impulse of Hall thrusters are well adapted for north–south station keeping of geostationary telecommunications satellites. The French space agency, Centre National d'Etudes Spatiales will launch an experimental telecom satellite Stentor with two Hall thrusters: PPS-1350 and SPT-100.[1] New programs involving SPTs are also under consideration. First, Hall thrusters are being considered for telecommunications constellations in low Earth orbit (the Skybridge program).[2] A Hall thruster, the PPS-1350, will be used for the Earth–moon transfer of Smart1 ESA horizons 2000 scientific program.[2]

For these new applications, both larger and smaller devices are required. In parallel to experimental investigations, numerical models can help explain and optimize the physical processes in Hall thrusters.[3–6] One-dimensional transient-hybrid models of the SPT-100 acceleration channel have been developed recently.[5,6] The primary components of the model we have developed[5] include the continuity equation for neutrals with a constant velocity and ionization loss term, a microscopic description of the ion transport, and a fluid description of electrons. Charge neutrality is assumed, and the axial distribution of the radial magnetic field profile is given. The model successfully predicted the plasma oscillations observed in this device.[7] The predictions of this simple quasi-neutral hybrid model have been qualitatively validated with a more accurate one-dimensional particle-in-cell (PIC) Monte Carlo collision model.[8] A number of improvements to the model have been added including a particle model of ion transport and doubly charged ions to examine their effect on performance of the SPT-100.

In this paper, we focus on the prediction of the performance of a SPT-100 with the one-dimensional model. We describe, first, the approximations and governing equations of the model; the numerical techniques and data are discussed next. Then we define the performance of the Hall thruster. The calculations of the performance as a function of voltage and mass flow rate of xenon and krypton for a SPT-100 are presented in detail and compared with experimental results. Last are some brief conclusions.

Approximations and Governing Equations

The one-dimensional hybrid model is based on the same assumptions as the model of Ref. 5. In the present work doubly charged ions are included in the simulations. This group of ions is treated in the same manner as the singly direct ionization of atoms. We use a creation source term corresponding to direct electron impact double ionization from the ground state of xenon and krypton atoms. The contribution of stepwise ionization (electron impact of Xe^+ leading to Xe^{++} and Kr^+ leading to Kr^{++}) is also included. We neglect the effect of triply charged ions because the thresholds of ionization from ground state are 70 and 90 eV for xenon and krypton,[9] respectively. The ion transport of singly and doubly charged particles is described by following the trajectories of a sample of ions (PIC model) rather than by solving numerically the Vlasov equation as in Ref. 5.

The assumptions of the model are as follows. 1) There is quasi neutrality of the plasma. 2) Ion transport is described with a one dimension in space and velocity collisionless PIC method. 3) The electric field is obtained from the current density, using the electron momentum equation. 4) The electron mobility perpendicular to the magnetic field is classical and includes the effects of electron–neutral collisions as well as electron–wall collisions (in a phenomenological way). 5) The electron distribution function is Maxwellian, the electron mean energy being obtained from a simplified energy equation.

The hybrid model is, therefore, based on the following equations. The effect of the magnetic field is negligible for the ions, and so the ion transport equation is given by

$$\frac{\partial f_i^\alpha}{\partial t} + v_x \frac{\partial f_i^\alpha}{\partial x} + \frac{Z_{\alpha^e}}{M} E \frac{\partial f_i^\alpha}{\partial v_x} = C^\alpha \tag{1}$$

the right-hand term in Eq. (1) takes into account the creation of ions by a source term of direct ionization of the ground state. This source term $S^{g,\alpha}$ can be written as

$$S^{g,\alpha}(x,t) = n_p(x,t) N_a(x,t) k_i^{g,\alpha}(x,t) \tag{2}$$

All of the ions created from the ground state are created with the neutral atom velocity v_0. C^α includes also the effect of stepwise ionization, with a lost term of single ions in the transport equation for single-charged ions, and a source term of creation of double ions in the doubly charged ions transport equation. A Monte Carlo method is used to estimate this effect and is detailed subsequently. The resolution of Eq. (1) gives the ion densities, velocities, and fluxes for each species α.

The plasma density is obtained with the assumption of quasi neutrality:

$$n_p(x,t) = \sum_\alpha n_i^\alpha(x,t) \tag{3}$$

The equation of continuity for the neutral atoms with constant velocity v_0 and a loss term due to direct ionization gives the neutral density:

$$\frac{\partial N_a(x,t)}{\partial t} + v_0 \frac{\partial N_a(x,t)}{\partial x} = -\sum_\alpha n_p(x,t) N_a(x,t) k_i^{g,\alpha}(x,t) \tag{4}$$

The neutral atom density in the anode plane is

$$N_a(0,t) = \Phi_0 / v_0 \tag{5}$$

where Φ_0 is the neutral flux at the anode plane deduced from the gas mass flow rate.

Because the plasma is supposed to be quasi neutral, the electric field is not obtained from Poisson's equation. The electric field is deduced from the electron momentum equation (with only the drift term) and from current continuity:

$$E(x,t) = -\sum_\alpha \frac{\varphi_i^\alpha(x,t)}{n_i^\alpha(x,t)\mu_e(x,t)} + \frac{J_T(t)}{n_p(x,t) e \mu_e(x,t)} \tag{6}$$

The ion fluxes and densities come from Eq. (1); the relation

$$V_d = -\int_0^d E(x,t)\,\mathrm{d}x \tag{7}$$

gives, with Eq. (8), the total current.

The electron mobility is described using the classical mobility in a transverse magnetic field:

$$\mu_e(x,t) = \frac{e}{m_e} \frac{\nu_m(x,t)}{\nu_m^2(x,t) + \omega_B^2(x)} \tag{8}$$

When the electrons ionize the neutrals in the region near the exhaust plane of the thruster, the neutral density decreases to zero. In this region of low neutral density, the typical maximum plasma density and electron temperature are 10^{12} cm^{-3} and 20 eV, respectively. If we estimate the electron–ion collisions frequency, we obtain an electron–ion collision frequency of 10^5 s^{-1} with an electron–ion cross section given by the Coulomb approximation.[10] The electron energy is large enough that the electron–ion collisions are negligible (the Coulomb cross section varies as $1/T_e^2$). The electron–ion collisions are not sufficient to permit the electron transport in the axial direction in the zone at the exit of the channel. In the exhaust region, the momentum exchange frequency decreases to zero and so does the electron conductivity. We do not obtain a stable solution for Eq. (6)[5] if no other assumption is made on the electron transport.

To make possible the electron transport in the direction perpendicular to the magnetic field even when the neutral density goes to zero, we have added to the electron collision frequency a contribution due to collisions with the walls. This near-wall conductivity was suggested by Russian research[11] to explain the anomalous electron transport in the SPT. We account for electron–wall collisions in the simulation by introducing a supplementary constant collision frequency.[5] It is difficult to estimate the electron–wall momentum interaction frequency $\nu_{\mathrm{wall},m}$. It is clear that the electron–wall collision frequency depends of the electron energy, which varies axially

but also depends of the unknown axial profile of the Debye potential V_D. In this conditions it is difficult to predict the real variation of the electron–wall collision frequency as a function of the axial profile. We adjusted this frequency to obtain a calculated current in reasonable agreement with the experimental results.[12] In the results presented later, the electron–wall frequency is constant in the entire channel and has a value of 2×10^6 s^{-1}. This value permits us to successfully compare calculations and experimental results concerning the influence of the applied potential on the current (shape and amplitude of the oscillations) for an SPT-100-ML.[13]

The electron mean energy is obtained from the following simplified energy equation:

$$\frac{5}{3}\frac{\partial \overline{\varepsilon_e}(x,t)}{\partial x} = -eE(x,t) + \frac{\overline{\nu_\varepsilon}(x,t)}{\overline{\nu_e}(x,t)}\overline{\varepsilon_e}(x,t) \tag{9}$$

with an energy gain term due to the electric field and a loss term due to electron–atom and electron–single ion collisions and to the electron secondary emission by electron impact. The electron–atom energy losses correspond to inelastic processes including ionization (single and double). The electron–ion energy losses come from the ionization of single-charged ions. We take into account the effect of the secondary electron emission by electron impact in a phenomenological way (more details may be found in Ref. 5).

We discuss next the numerical techniques and the data we used to solve this set of equations.

Data and Numerical Techniques

The numerical technique requires the excitation, ionization (single and double), and momentum exchange cross sections by electron impact on xenon and krypton atoms. Also needed is the ionization cross section of Xe^+ and Kr^+ leading to Xe^{++} and to Kr^{++}, respectively, by electron impact. The inelastic cross sections (excitation and ionization) are included in the electron energy loss frequency of Eq. (9). The ionization cross sections of the ground state are used to estimate the ion production rates of Eq. (2) and the loss term of neutral atoms in Eq. (4). The stepwise ionization cross sections are used to estimate the stepwise ionization rate. The momentum exchange cross section is used in the electron mobility [Eq. (8)]. The inelastic cross sections (single direct ionization and excitation) come from Puech and Mizzi[14] for xenon and from data of Date et al.[15] for electron impact on krypton. The doubly direct ionization cross sections from the ground state (for xenon and krypton) come from Wetzel et al.[9] The cross sections for ionization of Xe^+ and Kr^+ are deduced from Achenbach et al.[16] and Defrance et al.[17] Ionization and energy loss rates are obtained by assuming that the electron distribution function is Maxwellian. A comparison of the ionization rates k_i^+ and $k_i^{g,\alpha}$ and energy loss rates k_ε^+ and k_ε^g in xenon and krypton are given in Figs. 1 and 2, where k_i^+ and $k_i^{g,\alpha}$ are, respectively, the stepwise ionization rate and the direct ionization rates from the ground state ($\alpha = 1$ for single direct ionization and $\alpha = 2$ for double direct ionization). The energy loss rate for ionization of a single ion is k_ε^+, and the total energy loss rate for electron–atom collisions is

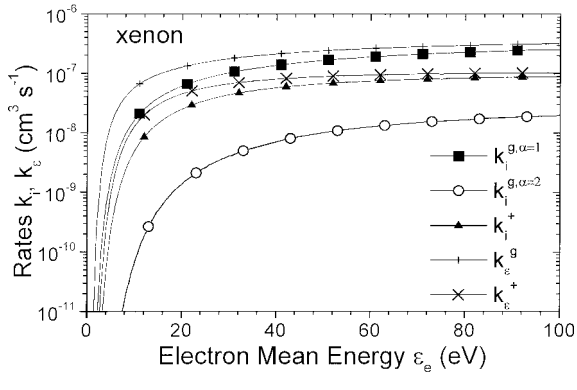

Fig. 1 Ionization and energy loss rates calculated with a Maxwellian electron distribution function in xenon.

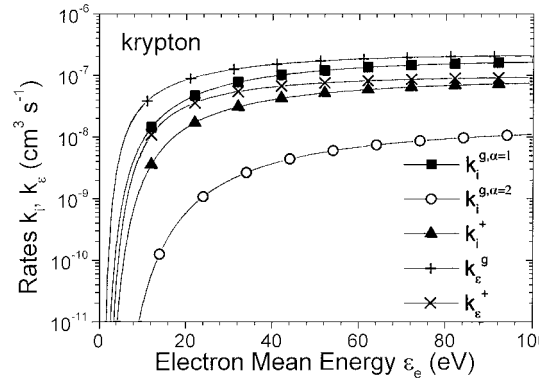

Fig. 2 Ionization and energy loss rates calculated with a Maxwellian electron distribution function in krypton.

k_ε^g. The momentum exchange rate k_m is estimated to be 2.5×10^{-13} and 2.0×10^{-13} m^{3}s^{-1} for xenon and krypton, respectively.

Equation (9) is solved using a classical fourth-order Runge–Kutta method (see Ref. 18). We use an upwind scheme to solve Eq. (4).[19] In the model of Ref. 5, Eq. (1) was solved with an upwind scheme and a time-splitting method. The upwind scheme is a simple method but rather diffusive.[20] In the calculations presented here, we used a Monte Carlo particle method to describe the collisonless ion transport.

The channel is divided into cells. As in the PIC technique,[21] we consider macroparticles, where each macroparticle represents a large number of ions (more than 10^7). The trajectory of a test particle number l is integrated using Newton's law:

$$\frac{d\boldsymbol{r}_l}{dt} = \boldsymbol{v}_l, \qquad M\frac{d\boldsymbol{v}_l}{dt} = Z_\alpha e\boldsymbol{E} \tag{10}$$

The classic leap-frog scheme is used for the resolution of these equations.[22]

At each time step Δt of the ion motion, some macroparticles are created in each grid cell depending on the ion production rate S_j^α of the species considered. The number of test particles created in each cell is determined as follows:

$$N_j^\alpha = \left(S_j^\alpha \Big/ S_{\max}^\alpha\right) N_s^\alpha + N_m^\alpha \tag{11}$$

The first term is directly proportional to the production rate. The difficulty comes from the difference between the maximal and the minimal production rates (a factor of 10^4 or more). The second term permits us to keep a minimum number of particles in each cell and to avoid a null ion density in a cell. A weight is assigned to the macroparticle l proportional to the ion production rate S_j^α and inversely proportional to the number of simulated ions created in the cell N_j^α:

$$w_l = S_j^\alpha \Delta t \Big/ N_j^\alpha \tag{12}$$

Random numbers are used to distribute the test particles uniformly in the cell. The velocity of the macroparticles created by ionization is v_0 for ionization of atoms from ground state.

To limit the total number of ions in the simulation we use the following procedure. The N_j^α ions are created during a time interval Δt, which does not necessarily coincide with the integration time step of the ion trajectories but can be larger. The Δt for ion generation is chosen large enough so that the total number of simulated ions leaving the device during this time interval is slightly larger than the total number of simulated ions generated by ionization. This avoids the random elimination of low-weight macroparticles (e.g., see Ref. 23).

To take into account the stepwise ionization by electron impact on singly charged ions, after the integration of a single particle test l during Δt, a probability of collision P_c is estimated. In our case, $P_c \ll 1$, so this probability can be simply written as

$$P_c = \nu_i^+ \Delta t \tag{13}$$

with $\nu_i^+ = n_p k_i^+$. P_c is compared with a pseudorandom number r_a uniformly weighted between 0 and 1. If $r_a \geq P_c$, then ionization occurs, and a new double ion test particle of weight w_l is created with the velocity and the position of the test particle l.

The ion density is calculated on the nodes of the grid by a simple linear-weighting scheme.[24] The mean velocities and fluxes of each species of ion are also estimated on the nodes of the grid. The ion mean velocities make it possible to deduce the velocity of the ion beam [Eq. (14)], and the ion fluxes are used for the calculation of the electric field [Eq. (6)] and to obtain the thrust of the SPT [Eq. (14)].

In the calculations presented in this paper, typically 25,000 test particles are used. The computational time is 2 h on a 400-MHz personal computer to simulate 400 μs.

Comments on the Boundary Conditions

As mentioned in Ref. 5, the results of the model are dependent on the boundary conditions for the ion density at the anode. We impose a nonzero ion flux and an ion velocity equal to v_0 at the anode. In the results presented in this paper we impose an ion density of 10^{11} cm^{-3} next to the anode. A parametric study has shown that values of this imposed ion density larger or equal to 10^{11} cm^{-3} does not strongly affect the total current of the discharge in the exit plane. This supplementary current is then on the order of few milliampere (which is low comparing to the 4 A of the total current). If a much lower ion density at the anode is used, then a large anode electric field develops in the anode region and the model does not give realistic results. This problem is partly due to the quasi-neutrality assumption and to that the calculated electric field [see Eq. (6)] goes to infinity when the plasma density goes to zero. The simulation of this region has been simplified neglecting the diffusion term in the electron momentum equation. In this region of low electric field, the diffusion term can permit an inversion of the electric field and then a sustainment of the plasma as observed in PIC simulations of Hall thrusters.[8] We also underestimate the density of the atoms in the region at the end of the injector typically by a factor of 10 due to the small area of the injector hole. The plasma density is then also underestimated in this region due to the underestimation of the ionization source term. Work is underway to improve the model description in the anode region.

Hall Thruster Performance

The thrust, the specific impulse, and the total efficiency characterize the performance of the SPT. The thrust T, in newtons, represents the reaction force to the expansion of the propellant mass. The specific impulse I_{sp}, expressed in seconds, is the duration for which the thruster can provide a thrust of 10 N with 1 kg of propellant.

We have neglected the effects of neutrals in calculating the thrust because they have a negligible velocity compared to that of ions. Thus the thrust is the sum of the product of the ion mass flow rate at the thruster exhaust multiplied by the ion exhaust mean velocity for each species:

$$T = \sum_\alpha T_i^\alpha = \sum_\alpha \dot{m}_i^\alpha v_i^\alpha \tag{14}$$

where the ion mass flow rate can be expressed as a function of the ion flux at the exhaust of the SPT

$$\dot{m}_i^\alpha = MA\varphi_i^\alpha \tag{15}$$

The specific impulse is deduced from the thrust:

$$I_{sp} = T/\dot{m}g \tag{16}$$

and the total efficiency of the thruster, with $P_d = J_d V_d$, can be written as

$$\eta = T^2 \Big/ 2\dot{m} P_d \tag{17}$$

The acceleration efficiency η_a is given by

$$\eta_a = J_i / J_d \tag{18}$$

and the propellant efficiency η_u (giving the ionized fraction of the neutral mass at the exhaust) is

$$\eta_i = \sum_\alpha \dot{m}_i^\alpha \Big/ \dot{m} \tag{19}$$

We can define the beam energy efficiency by the relation

$$\eta_E = \varepsilon_b / eU_d \tag{20}$$

We can also describe the global efficiency as in the case with only singly charged ions with the expression[25]

$$\eta = \eta_u \eta_a \eta_E \gamma^2 \tag{21}$$

The thrust loss factor γ includes exhaust beam divergence and profile losses.[3]

Then, from relations (17–21), we can deduce the beam energy efficiency η_E with singly and doubly charged ions:

$$\eta_E = \eta \Big/ \eta_a \eta_u \gamma^2 = \varepsilon_b / eU_d \tag{22}$$

with

$$\varepsilon_b = \frac{M v_i^{\alpha=1^2}}{2} \left\{ \frac{(1+\beta_T)^2}{(1+2\beta_\varphi)(1+\beta_\varphi)} \right\} \tag{23}$$

writing $\beta_T = T_i^{\alpha=2} / T_i^{\alpha=1}$ and $\beta_\varphi = \varphi_i^{\alpha=2} / \varphi_i^{\alpha=1}$.

If the doubly charged ions are neglected, we obtain the classical formula

$$\varepsilon_b = M v_i^{\alpha=1^2} \Big/ 2 \tag{24}$$

Results and Discussion

We performed calculations to study the effects of the propellant composition (xenon vs krypton), of the applied voltage and of the mass flow rate on the performance of a Hall thruster. The simulated device is the SPT-100-ML. This SPT-100 Hall thruster has been tested in the Propulsion Ionique pour Vols Orbitaux, Interprétation et Nouvelles Expériences (PIVOINE) facility. More details on the design of this thruster and on the PIVOINE facility are found by Béchu et al.[26]

The axial profile of the radial magnetic field used in all of the calculations is shown in Fig. 3. The cross section area of the thruster, A, is 40 cm^2.

The neutral atoms are injected with a velocity of 3×10^4 cm/s in the case of xenon and 3.76×10^4 cm/s in the case of krypton, to keep the same thermal energy of the emitted atoms.

The SPT produces spontaneous oscillations of the current.[7] The performance of the thruster also oscillates in time and all of the results presented in this paper are averaged in time.

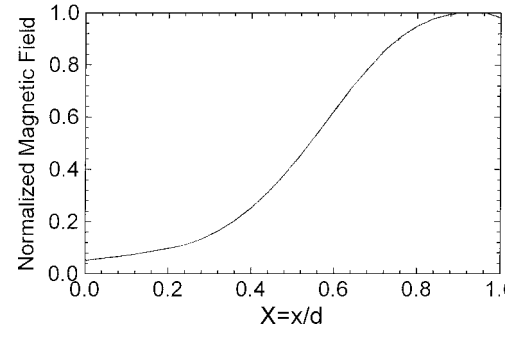

Fig. 3 Axial distribution of the radial magnetic field used for the simulations; anode is at $x = 0$ and the exhaust at $x = d$.

Table 1 Calculated efficiency of the SPT100-ML for 5 mg/s of xenon and for different discharge voltages

V_d, V	η_u, %	η_a, %	η_E, %	η, %
150	44.1	95.6	50.5	21.3
200	72.5	96.5	46.0	32.2
250	85.5	95.5	46.1	37.6
300	89.7	96.3	47.6	41.0
350	94.4	95.6	43.0	38.8
400	96.6	95.3	40.0	36.8

Calculations for Xenon

We present in Table 1 the efficiencies for applied voltage in the range 150–400 V for a xenon mass flow rate of 5 mg/s at the anode. As shown in Table 1, the thrust efficiency increases with the applied voltage, with a peak for a voltage of 300 V. In the one-dimensional model, neither the ion beam divergence nor the ion losses to the wall are taken into account, and the γ factor is, therefore, set to 1 [see Eq. (21)]. In the acceleration zone, where the magnetic field is large, the electric field must increase to compensate for the low electron mobility. The ions are accelerated by this electric field toward the exhaust.[5] It is clear that, to minimize ion recombination on the walls, the acceleration channel length should be kept short. Our model can not, however, properly describe this aspect because ion losses to the walls are not considered. The ion loss on the wall chamber in an SPT is relatively low compared with the ion losses on the grid of an electrostatic ion thruster.[25]

We note that the acceleration efficiency is relatively insensitive to the applied voltage, at around 95%. A similar behavior of the acceleration efficiency as a function of the applied voltage has been observed experimentally on a 70-mm thruster with a boron nitride channel.[27] The experimental current ratio J_i/J_d varies from 64 to 67% for two xenon mass flow rates (1.04 and 1.53 mg/s) and for voltage between 150 and 500 V. We also note that beam energy efficiency decreases with the applied voltage. Some experimental results of the beam efficiency reach a value around 75% (Ref. 28). We underestimated this value in our calculations (see Table 1) mainly due to the strong oscillations of the thruster. In this range of voltage, and for large enough magnetic field in the anode region, some oscillations with a frequency around 100 kHz appear. The high-frequency oscillations are associated with a maximum of electric field moving at a high speed from the anode to the acceleration zone.[8] The distribution of the ionization source term in the channel is correlated with the maximum of electric field. Calculations of time average spatial distribution of the ionization source term show a repartition spread out in a zone crossing the drop of the electric potential. A significant fraction of the ions are created between the middle and the end of the thruster channel. The ion beam average energy is strongly affected by the ions created on the last centimeter of the thruster, which are accelerated by only a part of the applied potential.

Calculations of electron transport have shown that the electron distribution function is not Maxwellian due to the effect of secondary electron emission by electron impact on ceramics in Hall thrusters (see Ref. 29). Work is underway to have a better description of the electron distribution function to better estimate the ionization rate that influences the calculation of the source term [Eq. (2)]. Effects such as the magnetic field in the region outside of the thruster, which still have nonnegligible values giving an accelerating electric field out of the channel as observed by laser-induced fluorescence preliminary measurements on the SPT-100-ML thruster,[30] is also a way to improve the modeling of the ion beam.

The total efficiency depends strongly on the propellant efficiency (see Table 1). When the voltage is low, the ionization of the neutral flux is incomplete. For large values of the applied voltage, the fraction of the neutral flux that is ionized by electrons can be as large as 97% in the calculations (see Table 1, where η_u is 96.6% for a channel voltage of 400 V). The strong influence of the propellant efficiency on the total efficiency has been observed experimentally on Israeli and Japanese Hall thrusters.[27,31]

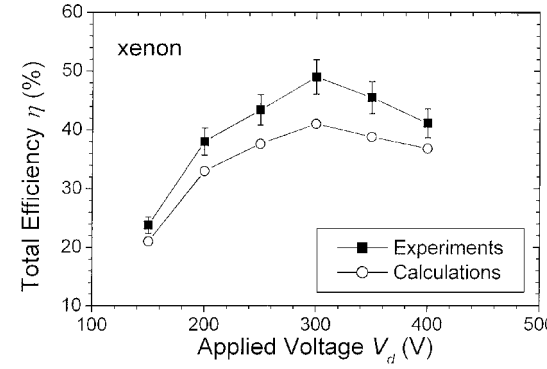

Fig. 4 Total efficiency as a function of discharge voltage; xenon mass flow rate is 5 mg/s: comparison between measurements[26] and calculations.

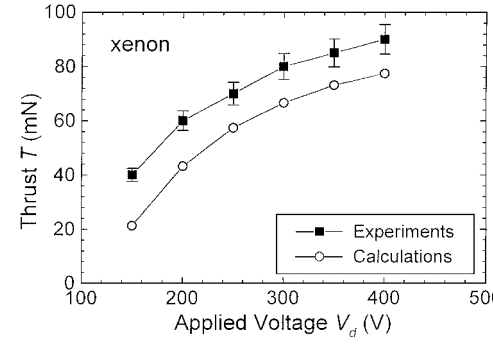

Fig. 5 Thrust as a function of discharge voltage; xenon mass flow rate is 5 mg/s: comparison between measurements[23] and calculations.

Figure 4 shows a comparison between calculations and experimental results. Note that no adjustment of the magnetic field, or other external parameters, is made to optimize the global efficiency of the SPT-100-ML in the experiment of Fig. 4. The thrust efficiency is maximum for a channel voltage of 300 V with a value of 50% in the experiments and 40% in the simulation. For larger voltages, the engine efficiency decreases due to the decrease of η_E in the calculations. Results obtained by the model underpredict the thrust of the SPT-100-ML (by 14–50% for xenon and 8–30% for krypton, see next paragraph). We have neglected in our model ionization mechanisms other than direct ionization (from ground or singly ionized states). The effect of ionization of excited states on the ion current and on the propellant efficiency could be important. We have also neglected the dissipated power in the magnetic coils and in the heating of the hollow cathode. This power dissipation could be nonnegligible at low voltages.

Figure 5 shows the variation of the thrust for discharge voltages between 150 and 400 V. As expected, the thrust increases with the applied voltage. The difference between experiments and calculations is around 15 mN.

SPTs are attractive because they are efficient within the optimum range of specific impulse for station keeping of satellites (1000–2000 s) (Ref. 25). We obtain a specific impulse of 1500 s for an applied voltage of 350 V in the simulation, and 1700 s is obtained in the experiments.[26]

Finally, Fig. 6 shows the total thrust efficiency as a function of the thrust. The maximum calculated efficiency is about 10% less than the measured one and is obtained for a thrust around 75 mN, that is 15 mN less than the thrust at maximum efficiency in the experiment. For high thrust, the global efficiency decreases, as observed in other SPTs.[31]

The results of calculation of the fractions of the different currents are summarized in Table 2. $J_i^{\alpha=1}$ represents the ion current of single-charged ions and $J_i^{\alpha=2}$ is the doubly charged ion current (sum of the ion currents coming from the ionization of ground state and of single-charged ions). As can be seen, the total ion current increases

Table 2 Calculated ion currents for 5 mg/s of xenon and for different discharge voltages

V_d, V	$J_i^{\alpha=1}$, %	$J_i^{\alpha=2}$, %	J_i, A
150	95.6	4.4	1.7
200	91.8	8.2	2.8
250	89.0	11.0	3.3
300	88.9	11.1	3.5
350	85.7	14.3	3.8
400	84.0	16.0	3.9

Table 3 Efficiencies obtained with the one-dimensional hybrid model for xenon and a discharge voltage of 300 V

$\dot{m}$, mg/s	η_u, %	η_a, %	η_E, %	η, %
3.0	74.3	96.4	44.3	31.7
4.0	81.6	96.0	47.2	37.0
5.0	89.7	96.0	47.6	41.0
6.0	95.1	95.6	49.3	44.8
7.0	95.1	95.3	51.1	46.3

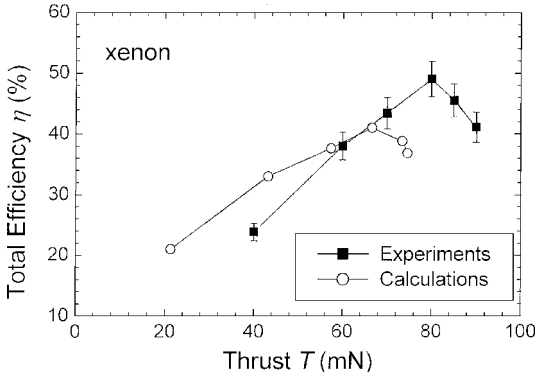

Fig. 6 Total efficiency as a function of thrust.

as the voltage increases. This behavior is due to the increase of the ionization efficiency (see Table 1). Note that the fraction of Xe^+ decreases from 95.6 to 84.0% when the voltage varies from 150 to 400 V. The fraction of Xe^{++} as expected increases with the voltage (4.4–16%). Around 50% of the Xe^{++} current comes from stepwise ionization of Xe^+; the contribution of doubly charged ions in these conditions is low, only few millinewtons on the total thrust. It does not explain the underestimation of the calculated thrust compared to measurements. The difference in magnitude between the ionization rate of the ground state and that of stepwise ionization (see Fig. 1) is compensated for by the difference between the atom and ion single-charge densities.

We also studied the influence of the mass flow rate on the thruster performance for a constant channel voltage of 300 V (see Table 3). The engine efficiency increases with the mass flow rate. The fraction of the doubly charged ion current is quasi constant (around 12% of the total current) in the range of mass flow rate studied. The beam energy efficiency is due to the strong oscillations of the distribution of the potential inside the channel and to the repartition of the source term in the channel. The acceleration efficiency is not very sensitive to the increase of the mass flow rate of xenon. The propellant efficiency increases with the mass flow rate. This is because the source terms of production of ions are improved when the density of the propellant increases [see Eq. (2)]. The propellant efficiency reaches 95% for $\dot{m} = 6$–7 mg/s, and η reaches a value around 46%. Experimental results from Raitses et al.[32] give both specific impulse and thruster efficiency increasing with the mass flow rate, for a 70-mm thruster of a channel length of 2 cm, for a voltage of 300 V, and for xenon flow rate in the range 1–2.2 mg/s.

Figure 7 shows the thrust and the input power for a xenon mass flow rate between 3 and 7 mg/s. We can see a quasi-linear variation of

Table 4 Calculated efficiencies for 5 mg/s of krypton

V_d, V	η_u, %	η_a, %	η_E, %	η, %
200	45.4	96.6	44.1	19.3
250	66.3	97.2	40.8	26.3
300	75.8	97.4	39.3	29.0
350	84.3	97.0	36.7	30.0
400	85.3	96.8	33.3	27.5

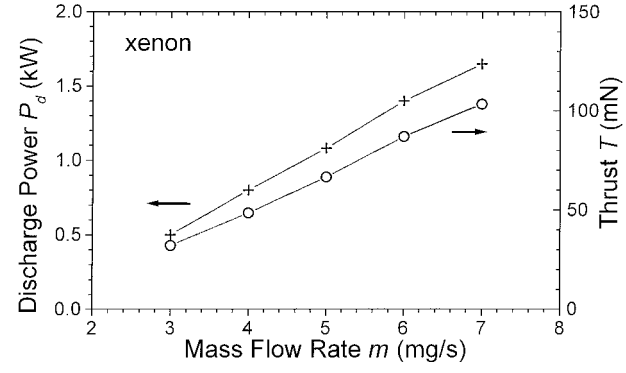

Fig. 7 Discharge power and thrust as a function of mass flow rate for 300 V.

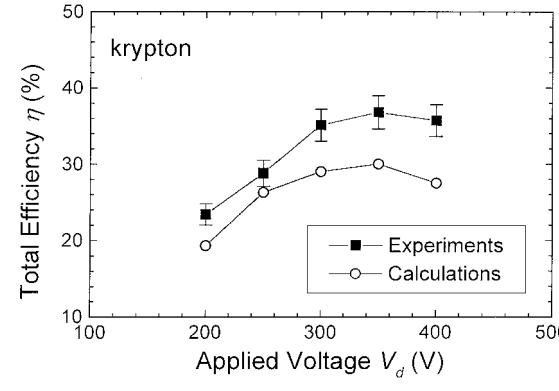

Fig. 8 Total efficiency as a function of discharge voltage in the SPT-100-ML in krypton; krypton mass flow rate is 5 mg/s: comparison between measurements[26] and calculations.

the thrust with the mass flow rate. This linear behavior of the thrust as a function of the mass flow rate has been observed experimentally for different Hall thrusters, such as for small SPT[33] and for a laboratory Hall thruster studied in Israel,[34] for example.

For $\dot{m} = 7$ mg/s, the thrust reaches 100 mN, but we also see that the discharge power is rather large, on the order of 1.7 kW. The ion total current is on the order of 1.7 A for 3 mg/s and reaches 5.5 A for 7 mg/s.

Calculations for Krypton

Table 4 shows the performance of the SPT-100-ML with a 5-mg/s flow rate of krypton and can be compared with Table 1 corresponding to xenon. The total efficiency is also represented as a function of voltage in Fig. 8 for krypton.

The behaviors of the acceleration and beam energy efficiencies compared to the xenon case are the same. As in the xenon case, the voltage strongly influences the propellant efficiency η_u. Experimental results of Komurasaki and Arakawa[31] show that the propellant efficiency of xenon is about two times larger than that of argon. These experimental results were obtained for voltage that ranged from 100 to 250 V and for a lower mass flow rate than our case (less than 2 mg/s). The higher propellant efficiency of xenon is related to its larger ionization rate (Figs. 1 and 2). Moreover, the neutral atom density is lower for Xe than for Kr (it varies as $1/\sqrt{M}$). We

Table 5 Efficiencies obtained with the one-dimensional hybrid model for krypton as a function of mass flow rate for a discharge voltage of 300 V

$\dot{m}$, mg/s	η_u, %	η_a, %	η_E, %	η, %
3.0	47.5	97.4	40.2	18.6
4.0	64.7	97.6	36.6	23.1
5.0	77.4	97.4	37.0	27.9
6.0	82.8	97.3	38.9	31.4
7.0	86.5	97.1	41.4	34.7

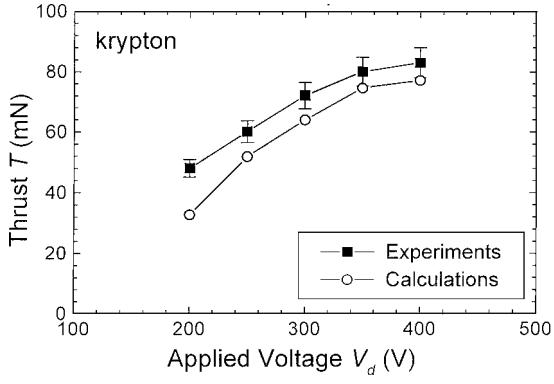

Fig. 9 Thrust as a function of discharge voltage; krypton mass flow rate is 5 mg/s: comparison between measurements[26] and calculations.

have kept the same neutral flow rates at the anode to compare our calculations to the experimental results. In the case of krypton, the global efficiency increases with the voltage to a maximum efficiency of about 30% (compared with 40% for xenon). Brophy et al.[25] obtained for krypton a global efficiency of 38% for a SPT-100 with a voltage of 300 V and a flow rate of 4.23 mg/s. Measurements on the D-100 (an anode layer thruster built in Russia and tested at the University of Michigan for krypton[34]) of the total efficiency and specific impulse give the same behavior as our calculations. For the D-100, the maximum efficiency for a krypton mass flow rate of 9.3 mg/s is around 35% for a voltage of 300 V, and the specific impulse is 1450 s (Ref. 35).

The variations of the thrust with voltage shown in Fig. 9 show that krypton and xenon exhibit similar behavior. Brophy et al.[25] give similar (experimental) results for an SPT-100 in krypton at 300 V, 4.23 mg/s: 65-mN thrust and 1580-s specific impulse. Note that, in the range of voltage studied, the thrust increases, in contrast to the behavior of the total efficiency at high voltage. This is because the beam velocity and the propellant efficiency (see Table 4) are still increasing with the voltage in the considered range. The I_{sp} is on the order of 1300 s for $V = 300$ V and 1580 s for 400 V.

The total ion current varies between 2.7 A for 200 V up to 5.4 A for 400 V. The fraction of doubly charged ion current increases from 5.3 to 11.4% in the same range of voltage. The influence of the anode mass flow on the calculated performance of the SPT-100-ML in krypton can be seen in Table 5. We see, again, the same behaviors for the beam energy and acceleration efficiencies for krypton and for xenon. The propellant and engine efficiencies in krypton are smaller than in xenon as expected. The thrust increases linearly with the mass flow rate, with a value of 24 mN for $\dot{m} = 3$ mg/s up to 105 mN for 7 mg/s. For $\dot{m} = 7$ mg/s, the discharge power is larger than in xenon (2.3 kW vs 1.7 kW for xenon). The ion current increased by a factor of 4.5 (1.7–7.6 A) when the mass flow rate increases from 3 to 7 mg/s.

Conclusions

We have used a one dimensional hybrid simple model to calculate the performance of an SPT-100 and its variations as a function of applied voltage and gas mass flow rate in xenon and krypton. Even if the model is not predictive due to parameters such as electron–wall collisions frequency or imposed ion density in the anode region, it correctly predicts trends performance.

The calculations show the strong influence of the voltage and the mass flow rate for xenon and krypton on the propellant utilization. The model predicts a thrust of around 75 mN in typical conditions (350 V, 5 mg/s) for an SPT-100 in xenon, a value about 10–15 mN lower than the measured one. The calculated thrust in krypton is on the order of 75 mN in the same conditions. The calculated efficiencies are on the order of 40 and 30% in xenon and krypton respectively, in reasonable agreement with the measured values (which are about 10% higher). The explanation of differences between the two gases comes from the higher ionization rate for xenon. The discrepancies between experiments and calculations are not due to the effect of doubly charged ions, which play a minor role as we can see. It seems that the contribution of ionization of excited states could play a more important role due to the low threshold of creation and ionization of these excited states.

Future work concerns a more refined modeling of the anode region with the diffusion term in the electron momentum equation and an extension of the computational domain taking into account the region of the nonnegligible magnetic field after the exit plane of the thruster.

Acknowledgments

This work was performed in the framework of the Groupement de Recherche Centre National de la Recherche Scientifique (CNRS)/Centre National d'Etudes Spatiales (CNES)/Société Nationale d'Etudes et de Constructionde Moteur d'Avion (SNECMA)/ Office National d'Etudes et de Recherches Aérospatiales (ONERA) 2232 "Propulsion à Plasma pour Systèmes Spatiaux." L. Garrigues wants also to acknowledge the financial support of CNES. The authors want to thank the Laboratoire d'Aéothermique, CNRS–UPR9020 in Orléans for sharing the experimental data.

References

[1]Cadiou, A., Lyszyk, M., and Dudeck, M., "Research and Development on Plasma Thrusters in France," International Electric Propulsion Conf., IEPC Paper 99-007, Oct. 1999.

[2]Saccoccia, G., "European Electric Propulsion Activities," AIAA Paper 99-2158, June 1999.

[3]Komurasaki, K., and Arakawa, Y., "Two-Dimensional Numerical Model of Plasma Flow in a Hall Thruster," *Journal of Propulsion and Power*, Vol. 11, No. 6, 1995, pp. 1317–1323.

[4]Fife, J. M., and Martinez-Sanchez, M., "Comparison of Results from Two-Dimensional Numerical SPT Model with Experiment," AIAA Paper 96-3197, July 1996.

[5]Boeuf, J. P., and Garrigues, L., "Low Frequency Oscillations in a Stationary Plasma Thruster," *Journal of Applied Physics*, Vol. 84, No. 7, 1998, pp. 3541–3554.

[6]Lentz, C. A., and Martinez-Sanchez, M., "Transient One Dimensional Numerical Simulations of Hall Thrusters," AIAA Paper 93-2491, July 1993.

[7]Darnon, F., Garrigues, L., Boeuf, J. P., Bouchoule, A., and Lyszyk, M., "Spontaneous Oscillations in a Hall Thruster," *IEEE Transactions on Plasma Science*, Vol. 27, No. 1, 1999, pp. 98, 99.

[8]Garrigues, L., Heron, A., Adam, J. C., and Boeuf, J. P., "Hybrid and PIC Models of Stationary Plasma Thruster," *Plasma Sources Science and Technology*, Vol. 9, No. 2, 2000, pp. 219–226.

[9]Wetzel, R. C., Baiocchi, F. A., Hayes, T. R., and Freund, R. S., "Absolute Cross Sections for Electron-Impact Ionization of the Rare-Gas Atoms by Fast-Neutral-Beam Method," *Physical Review A*, Vol. 35, No. 2, 1987, pp. 559–577.

[10]Raizer, Y. P., *Gas Discharge Physics*, Springer-Verlag, Heidelberg, Germany, 1991, Chap. 2.

[11]Bugrova, A. I., Morozov, A. I., and Kharchevnikov, V. K., "Experimental Investigation of Near-Wall Conductivity," *Soviet Journal of Plasma Physics*, Vol. 16, No. 12, 1990, pp. 849–856.

[12]Boeuf, J. P., Garrigues, L., and Pitchford, L. C., "Modeling of a Magnetized Plasma: The Stationary Plasma Thruster," *Electron Kinetics and Applications of Glow Discharges*, edited by U. Kortshagen and L. Tsendin, Plenum, New York, 1998, pp. 85–101.

[13]Garrigues, L., Pérot, C., Gascon, N., Béchu, S., Lasgorceix, P., Dudeck, M., and Boeuf, J. P., "Characteristics of the SPT100-ML Comparisons Between Experiments and Models," International Electric Propulsion Conf., IEPC Paper 99-102, Oct. 1999.

[14]Puech, V., and Mizzi, S., "Collision Cross Sections and Transport Parameters in Neon and Xenon," *Journal of Physics D: Applied Physics*, Vol. 24, No. 11, 1991, pp. 1974–1985.

[15]Date, H., Sakai, Y., and Tagashira, H., "Boltzmann Equation Analysis of Electron Collision Cross Sections and Swarm Parameters for Krypton," *Journal of Physics D: Applied Physics*, Vol. 22, No. 10, 1989, pp. 1478–1481.

[16]Achenbach, C., Muller, A., Salzborn, E., and Becker, R., "Single Ionization of Multiply Charged Xenon Ions by Electron Impact," *Journal of Physics B: Atomic and Molecular Physics*, Vol. 17, No. 7, 1984, pp. 1405–1425.

[17]Defrance, P., Duponchelle, M., and Moores, D. L., "Ionization of Atomic Ions by Electron Impact," *Atomic and Molecular Processes in Fusion Edge Plasmas*, edited by R. K. Janev, Plenum, New York, 1995, pp. 153–193.

[18]Press, W. H., Flannery, B. P., Teukolsky, S. A., and Vetterling, W. T., Numerical Recipes, Cambridge Univ. Press, New York, 1986, Chap. 15.

[19]Hirsh, C., *Numerical Computation of Internal and External Flows*, Vol. 1, Wiley, New York, 1989, Chap. 7.

[20]Garrigues, L., "Modélisation d'un Propulseur à Plasma Stationnaire pour Satellite," Ph.D. Dissertation, Centre de Physique des Plasmas et Applications de Toulouse, Univ. Paul Sabatier, Toulouse, France, 1998 (in French).

[21]Birdsall, C. K., "Particle-in-Cell Charged-Particle Simulations, Plus Monte Carlo Collisions with Neutral Atoms, PIC-MCC," *IEEE Transactions on Plasma Science*, Vol. 19, No. 2, 1991, pp. 65–85.

[22]Hockney, R. W., and Eastwood, J. W., *Computer Simulation Using Particles*, Adam Hilger, Bristol, England, U.K., 1988, Chap. 4.

[23]Fiala, A., Pitchford, L. C., and Boeuf, J. P., "Two-Dimensional, Hybrid Model of Low Pressure Glow Discharges," *Physical Review E*, Vol. 49, No. 6, 1994, pp. 5607–5622.

[24]Birdsall, C. K., and Langdon, A. B., *Plasma Physics Via Computer Simulation*, Adam Hilger, Bristol, England, U.K., 1991, Chap. 2.

[25]Brophy, J. R., Barnett, J. W., Sankovic, J. M., and Barnhart, D. A., "Performance of Stationary Plasma Thruster: SPT-100," AIAA Paper 92-3155, July 1992.

[26]Béchu, S., Pérot, C., Gascon, N., Lasgorceix, P., Hauser, A., and Dudeck, M., "Operating Mode Investigation of a Laboratory Stationary Plasma Thruster," AIAA Paper 99-2567, June 1999.

[27]Ashkenazy, J., Raitses, Y., and Appelbaum, G., "Parametric Studies of the Hall Current Plasma Thruster," *Physics of Plasma*, Vol. 5, No. 5, 1998, pp. 2055–2063.

[28]Pérot, C., Gascon, N., Béchu, S., Lasgorceix, P., Dudeck, M., Garrigues, L., and Boeuf, J. P., "Characterization of a Laboratory Hall Thruster with Electrical Probes and Comparisons with a 2D Hybrid PIC-MCC Model," AIAA Paper 99-2716, June 1999.

[29]Degond, P., Latocha, V., Garrigues, L., and Boeuf, J. P., "Electron Transport in Stationary Plasma Thrusters," *Transport Theory and Statistical Physics*, Vol. 27, No. 3–4, 1998, pp. 203, 221.

[30]Bouchoule, A., Darnon, F., Philippe-Kadlec, C., Prioul, M., Lyszyk, M., Magne, L., Pagnon, D., Roche, S., Touzeau, M., Béchu, S., Lasgorceix, P., Sadéghi, N., Dorval, N., Marque, J. P., and Bonnet, J., "Optical and Electrical Diagnostics of the Plume and of the Active Channel of Closed Electron Drift Plasma Thrusters," *Proceedings of the 15th Europhysics Conference on Atomic and Molecular Physics of Ionized Gases*, Vol. 24F, European Physical Society, Lillafured, Hungary, Aug. 2000, pp. 30–33; also *Plasma Sources Science and Technology* (submitted for publication).

[31]Komurasaki, K., and Arakawa, Y., "Hall Current Ion-Thruster Performance," *Journal of Propulsion and Power*, Vol. 8, No. 6, 1992, pp. 1212–1216.

[32]Raitses, Y., Ashkenazy, J., Appelbaum, G., and Guelman, M., "Propellant Utilization in Hall Thrusters," *Journal of Propulsion and Power*, Vol. 14, No. 2, 1998, pp. 247–253.

[33]Guerrini, G., Vesselovzorov, A. N., Bacal, M., and Pokrovsky, I. B., "Investigation of a Small, Closed Electron Drift, Stationary Plasma Thruster," *Review of Scientific Instruments*, Vol. 67, No. 3, 1996, pp. 990–992.

[34]Ashkenazy, J., Raitses, Y., and Appelbaum, G., "Investigation of a Laboratory Model Hall Thruster," AIAA Paper 95-2673, July 1995.

[35]Marrese, C. M., Haas, J. M., Domonkos, M. T., and Gallimore, A. D., "D-100 Performance and Plume Characterization on Krypton," AIAA Paper 96-2969, July 1996.